2010 IEEE International Conference on Robotics and Automation
Anchorage Convention District
May 3-8, 2010, Anchorage, Alaska, USA

# High-Fidelity Joint Drive System by Torque Feedback Control Using High Precision Linear Encoder

Tomohiro Kawakami, Ko Ayusawa, Hiroshi Kaminaga and Yoshihiko Nakamura

*Abstract*— **When robots cooperate with humans it is necessary for robots to move safely on sudden impact. Joint torque sensing is vital for robots to realize safe behavior and enhance physical performance. Firstly, this paper describes a new torque sensor with linear encoders which demonstrates electro magnetic noise immunity and is unaffected temperature changes. Secondly, we propose a friction compensation method using a disturbance observer to improve the positioning accuracy. In addition, we describe a torque feedback control method which scales down the motor inertia and enhances the joint flexibility. Experimental results of the proposed controller are presented.**

## I. Introduction

Joint flexibility is required for humanoid robots in order to safely execute cooperative tasks with humans. To achieve flexible joint motion, precise measurement of joint torque is important. Joint torque can be estimated from actuator inputs such as motor current. However, it is hard to deduce the error in the estimated joint torque, because the friction arisen in the transmission is difficult to model. It is thus desirable to measure the output torque directly, so the measurement is free from internal friction.

In general, output torque is measured with deformation of an elastic part in the joint. Godler et al.[1] developed the torque sensing method using strain gauges, which are cemented directly onto the flexspline of Harmonic Drive. This method has the advantage that an additional elastic component is not required for measurement, but it is difficult to measure joint torque because of the torque ripple generated by the gear rotation. Vischer et al.[2] and Tsetserukou et al.[3] measured deformation of an elastic body after the reduction with optical distance sensors. As measurement accuracy is in inverse proportion to sensor stiffness, low sensor stiffness is inevitable in order to achieve high measurement resolution, which leads to complicated joint dynamics. Hirzinger et al.[4] developed a torque sensor with high sensor stiffness and high measurement resolution using strain gauges. They also realized a torque control system of the manipulator with the developed torque sensor, but strain gauges break down easily and need to be cemented exactly by a specialist. In addition, the high stiffness of the sensor makes it difficult to improve signal-to-noise ratio, because strain gauges have high sensitivity to electro magnetic noise. Therefore, the method for precisely measuring minute deformations with high signal-to-noise ratio is required.

In recent years, high resolution linear optical encoders become commercially available. Noise immunity and measurement principle of linear encoders give an advantage to the joint torque measurement of humanoid robots; they are suitable to measure small distortions of the highly rigid elastic part of the sensor.

In this paper, we propose novel torque sensing method using linear encoders. Linear encoders can measure small distortion generated in the transmission of the joint precisely, and the sensor has enough stiffness and resolution to be applied in humanoid robots. We also evaluate the performance of the proposed sensor by testing it with friction observer[5], [6], [7] and joint torque feedback[8].

## II. Torque Encoder

### A. General methods of torque measurement

Torque sensor often measure deformation of an elastic body in a power transmission. When the power transmission consists of a motor and a gear, the elastic body is usually installed at the output of the gear. Joint models with torque sensors become complicated, because an elastic body is installed in the power transmission. The following design guides are demanded to ensure installing the torque sensor does not change the joint model.

1) The stiffness of the torque sensor is an order higher than that of the reducer.
2) The inertia between the reducer and the sensor is minimized.

It is preferable that the torque sensor is stiff enough, but there is an inverse relationship between the sensitivity and the stiffness. In particular, the reducers in some joints of humanoid robots are very rigid, because they need high-power actuators and reducers. In that case, the torque sensor must be very rigid not to lead to the complicated joint model. It is important to strike a balance between the sensitivity and the stiffness.

Then, there are two primary ways to measure deformation. One way is to measure the strain with strain gauges[4]. The feature of strain gauges is high resolution and accuracy, but high sensitivity to electro magnetic noise. The other way is to measure the displacement with magnetic sensors[9] and optical sensors[2], [10], [11]. These sensors have noise immunity, but lower resolution than strain gauges.

This research is supported by gIRT Foundation to Support Man and Aging Societyh under Special Coordination Funds for Promoting Science and Technology from MEXT.

T. Kawakami, K. Ayusawa, H. Kaminaga and Y. Nakamura are with the Department of Mechano-Informatics, University of Tokyo, 7-3-1 Hongo, Bunkyo-ku, 113-8656 Tokyo, Japan tomohiro, ayusawa, kaminaga, nakamura@ynl.t.u-tokyo.ac.jp

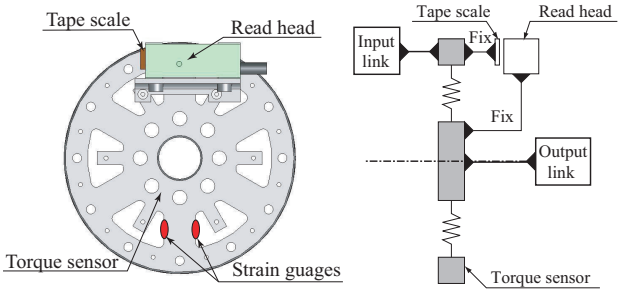


Fig. 1. Overview and conceptual diagram of 6-spoke torque sensor with encoder and strain gauges. The thickness is 8mm and the outside diameter is 88mm.

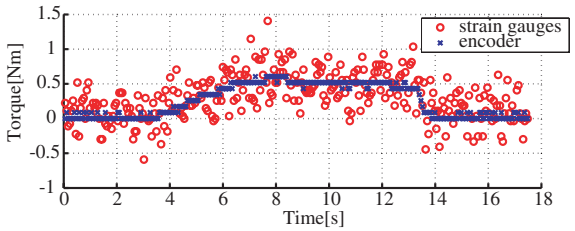


Fig. 2. Torque measurements with strain gauges and encoder under low load condition.

### B. Torque measurement with linear encoder

In this research, we digitally measure the displacement with linear optical encoders in place of analog sensors. Linear encoders are one of recent technologies and provides comparative sensitivity to strain gauges. These sensors have the following advantages in the torque measurement.

1) Excellent noise immunity to electro magnetic noise and temperature fluctuation.
2) Long-distance transmission is possible without signal deterioration.
3) The ability to improve the resolution without changing the stiffness of the sensor.

Where, we mention about 3). Strain gauges sensing relies on local strain sensing, linear encoders measure the total sum of distributed strain or displacement. Even if the strain occurred in the high rigid sensor is too tiny to be measured with strain gauges, linear encoders can measure the deformation when they are located properly, because of the difference of the measurement principle.

On the other hand, linear encoders measure all deformation including unexpected deformation such as plastic strain and slip of the fastened part in the measurement part. We thus demand the following designs of elastic parts in the sensor to improve the sensor performance.

1) The local concentration of stress is not caused easily in the measurement part.
2) The nonuniform deformation is not caused in the measurement part.

These demands are necessary to improve the repeatability and the linearity of the measurement.

### C. Comparison with strain gauges

We now compare the performance of linear encoders with strain gauges, using the torque sensor which has spokes as elastic parts shown in Fig. 1. This torque sensor has already been developed as 6-spoke torque sensor with strain gauges[12] and is changed to install both strain gauges and a linear encoder. Four strain gauges are cemented on the spoke of the torque sensor, which is red ellipsoidal area in Fig. 1. The resistance change of strain gauges is measured using a Wheatstone bridge on the immediate analog-digital converter board. Then, the linear encoder is an incremental encoder(Renishaw RGH24, resolution: 10[nm]). Torque measurement range is 200(Nm), torque resolution in case of the strain gauges is $3.7 \times 10^{-2}$(Nm), and that in case of the linear encoder is $8.6 \times 10^{-2}$(Nm). Fig.2 shows the simultaneous torque output with the strain gauges and with the linear encoder under low load condition. The standard deviation of the strain gauges is $2.3 \times 10^{-1}(\mathrm{Nm})$, that of the encoders is $5.5 \times 10^{-2}(\mathrm{Nm})$. This clearly shows that the encoders have better noise tolerance than the strain gauges.

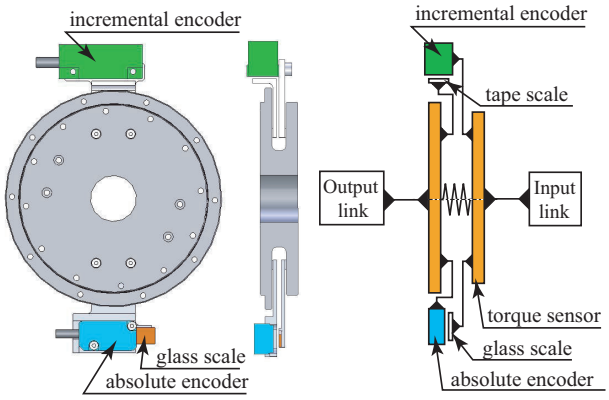


Fig. 3. Overview and conceptual diagram of Torque Encoder.

TABLE I
SPECIFICATON OF TORQUE ENCODER.

| | |
|---|---|
| Torsional stiffness of sensor | $3.0 \times 10^5(\mathrm{Nm/rad})$ |
| Torque measurement range | 200(Nm) |
| Outside diameter | 94(mm) |
| Thickness | 16(mm) |
| Safety factor | 9 |
| Material | Aluminium A7075 |

### D. Mechanism of Torque Encoder

The layouts of the developed torque sensor, which is specialized in measuring torque with encoders, are presented in Fig. 3, and its specification appears in Table I. This torque sensor is called "Torque Encoder" as follows. Torque Encoder is larger than the 6-spoke torque sensor, but its shape is so simple that the local concentration of stress is not caused easily in the measurement part. Torque Encoder has an incremental encoder and an absolute encoder (Nikon SAL-40A, resolution: 60[nm]). The linear encoders measure the relative angle between the two plates of Torque Encoder. Then, the torque resolution in case of the incremental encoder is $6.3 \times 10^{-2}$(Nm), and that in case of the absolute encoder is $3.2 \times 10^{-1}$(Nm). The torque resolution in case

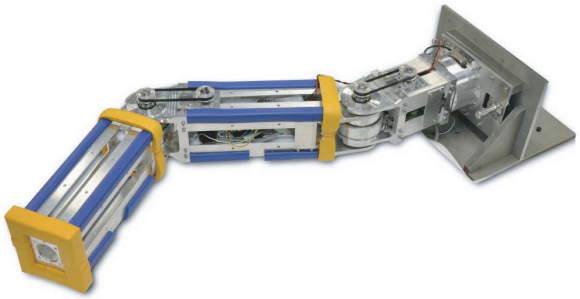

Fig. 4. The 3DoF torque controlled manipulator.

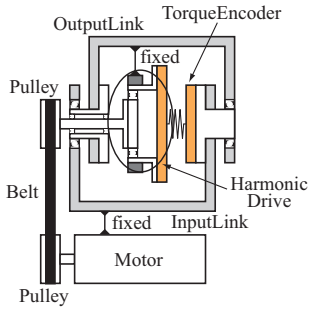


Fig. 5. Structure of the pitch joint.

of the absolute encoder is smaller than that in case of the incremental encoder, but the torque measurements with the absolute encoder can get the origin without measuring the zero offset at the time of startup.

### *E. Evaluation Experiments*

In this subsection, the performance of Torque Encoder is evaluated. We developed 3DoF torque controlled manipulator (Fig. 4). Torque Encoder was installed in each joint of the manipulator. Experiments were tested with the pitch joint (Fig. 5). Table II shows the main specification of this joint. Power transmission of this joint consists mainly of a brushless DC motor (Maxon EC-max40, 120W), Harmonic Drive (Harmonic Drives SHG20, reduction ratio: 100) and Torque Encoder. Against this joint system, the following two responses were measured.

**Exp. 1**: The response under load torque with fixed the joint.

**Exp. 2**: The response without fixing the joint.

In Exp. 1, to evaluate the hysteresis under high load torque, the load torque was applied on the output shaft of the gear and the input shaft of the gear is fixed. The load torque was continuously changed from $-160(\mathrm{Nm})$ to $160(\mathrm{Nm})$. The load torque was measured with a force gauge.

Fig. 6 shows the measurement error in case of each encoder. As the diagrams indicate, the hysteresis is $\pm 2(\mathrm{Nm})$ in the case of the incremental encoder and $\pm 3(\mathrm{Nm})$ in the case of the absolute encoder. The output of the incremental encoder is wave-like against the external torque. Since the output of the absolute encoder is not wave-like, it is quite

TABLE II

SPECIFICATON OF TORQUE SENSING JOINT.

| | |
|---|---|
| Actuator | Brushless DC Motor(120W) |
| Maximum output torque | 100(Nm) |
| No load speed | 60(rpm) |
| Reducer | Harmonic Drive Gear |
| Reduction ratio | 100 |

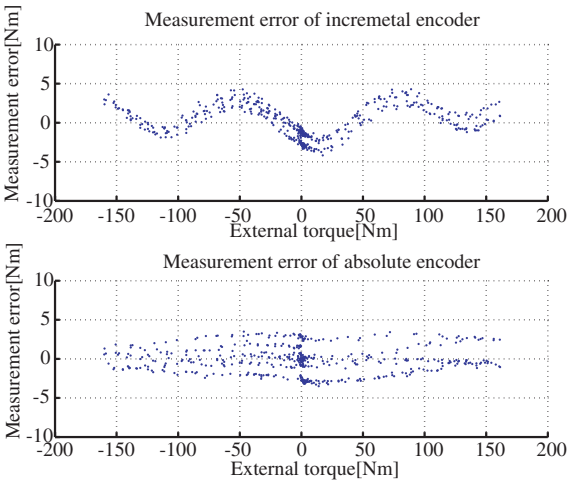


Fig. 6. Upper graph: Measurement error of external torque with incremental encoder. Lower graph: Measurement error of external torque with absolute encoder.

likely that the wave-like output is caused by the difference of the installation direction.

In Exp. 2, to evaluate the relationship between the joint angle and the torque, the torque was measured while changing the joint angle very slowly so as not to affect the torque. This experiment was performed in two ways. One way was to test with only the joint, the other way was to test with the joint connected to an arm and a weight. In Fig. 7, the upper graph is in the case of only the joint, and the lower graph is in the case of the joint with the arm. The input and output link are arranged linearly against the direction of the gravitational force at the starting point. In the case of only the joint, the torque offset which was about $\pm 2(\mathrm{Nm})$ was measured. On the other hand, the output in the case of the joint with the arm is equal to the sum of the ideal gravitational torque of the arm and the torque offset. The torque offset is compensated for by feedforward control, because the output is reproducible against the joint angle.

## III. DEVELOPMENT OF CONTROL SYSTEM FOR LOW IMPEDANCE JOINT

Because Torque Encoders have excellent noise immunity, it is possible for a control system with Torque Encoder to achieve rapid-response and high-gain torque feedback. This section describes a control system with Torque Encoder for realizing the low impedance joint by the friction compensation and the torque feedback control. Firstly, Fig. 8 shows the model of the torque sensing joint including a motor, a reducer, Torque Encoder and a link. The notation

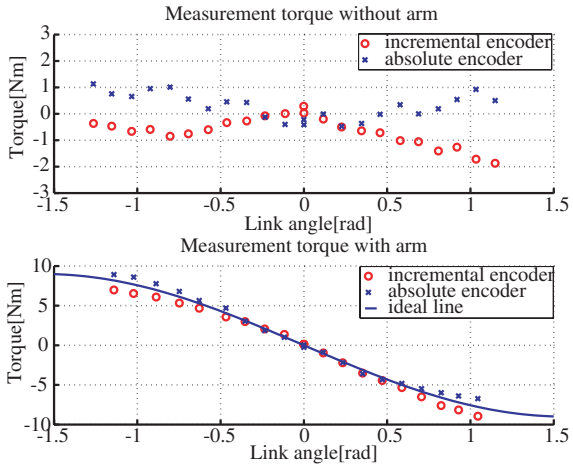


Fig. 7. Comparison of joint torque with and without arm.

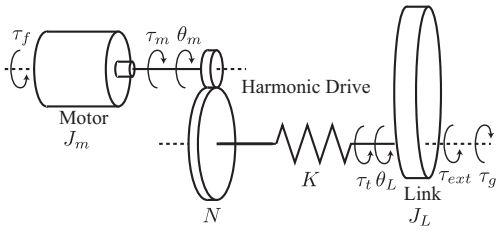


Fig. 8. The transmission model of the torque sensing joint.

of the parameter in Fig. 8 appears in Table III. The dynamic equations at motor side and link side are as follows:

$$J_L\ddot{\theta}_L + \tau_g(\theta_L) = \tau_t + \tau_{ext} \tag{1}$$

$$J_m\ddot{\theta}_m + \tau_f = \tau_m - \frac{1}{N}\tau_t \tag{2}$$

then,

$$\tau_t = K(\frac{\theta_m}{N} - \theta_L) \tag{3}$$

It is possible to consider the dynamics equations at motor side and link side separately in a joint with a torque sensor, as stated above. The controller is used for the above model to realize the low impedance joint as follows:

$$u_m = K_p(\theta_m^{ref} - \theta_m) - K_d\dot{\theta}_m + K_t(\tau_g - \tau_t) + \frac{1}{N}\tau_g \tag{4}$$

$$\tau_m = u_m + \hat{\tau}_f \tag{5}$$

where, $u_m$ is the output of the controller. In addition, $K_p, K_d$ and $K_t$ are positive feedback coefficients. $\theta_m^{ref}$ is the reference input of the motor angle and $\hat{\tau}_f$ is the friction estimate. In this article, the friction compensation is realized by the feedforward compensation of the friction estimated from the friction observer[5], [6], [7]. Additionally, reducing the virtual motor inertia $\tilde{J}_m$ for the driving system is realized by changing the torque feedback coefficient $K_t$[8].

The friction compensation of the motor and the gear is proposed by the disturbance observer in [5], [6], [7]. The

TABLE III
NOTATION OF PARAMETERS.

| | |
|---|---|
| $J_m$ | Motor side inertia |
| $J_L$ | Link side inertia |
| $\theta_m$ | Motor position |
| $\theta_L$ | Link position |
| $\tau_m$ | Motor torque |
| $\tau_f$ | Friction torque |
| $\tau_t$ | Joint torque |
| $\tau_{ext}$ | External torque |
| $\tau_g$ | Gravity torque |
| $K$ | Stiffness of joint |
| $N$ | Reduction ratio |

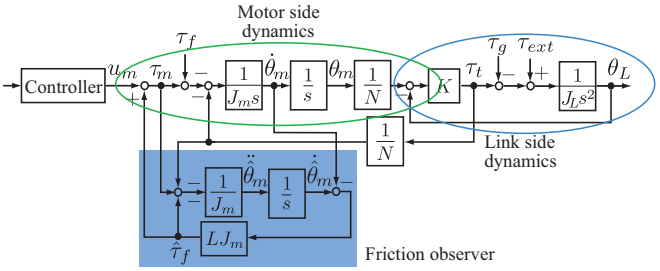


Fig. 9. Overview of the control system with friction observer.

observer dynamics are as follows:

$$\tau_m = J_m\ddot{\hat{\theta}}_m + \frac{1}{N}\tau_t + \hat{\tau}_f \tag{6}$$

$$\hat{\tau}_f = -LJ_m\left(\dot{\theta}_m - \dot{\hat{\theta}}_m\right) \tag{7}$$

where, $L$ is the design parameter of the observer, and $\dot{\hat{\theta}}_m$ if the state vector of the observer. The block diagram of the controller appears in Fig. 9. In short, the friction torque $\hat{\tau}_f$ can be estimated from the motor torque $\tau_m$, the motor velocity $\dot{\theta}_m$ and the joint torque $\tau_t$. Combining Eq.2, Eq.6 and Eq.7 by Laplace transform, the friction estimate $\hat{\tau}_f$ is derived as follows:

$$\hat{\tau}_f = \frac{1}{L^{-1}s + 1}\tau_f \tag{8}$$

$\hat{\tau}_f$ is equal to the output of the actual friction and the low-pass filter. In addition, $L^{-1}$ is the time constant of the low-pass filter. It is desirable to set $L$ to a large value for the improvement of responsiveness, but $\hat{\tau}_f$ often behaves in an unstable way. We need to set a suitable value to $L$. The friction compensation is realized by the feedforward compensation of the friction estimate.

Then, When we change the joint torque feedback coefficient $K_t$, the virtual motor inertia is changed [8], which is called inertial scaling as follows. Combining Eq.2 and Eq.5, the dynamic equations at motor side are as follows:

$$\tilde{J}_m\ddot{\theta}_m = \tilde{u}_m - \frac{1}{N}\tau_t \tag{9}$$

$$\tilde{J}_m = \frac{1}{1 + NK_t}J_m \tag{10}$$

Then it is based on the assumption that $\hat{\tau}_f$ is equal to $\tau_f$

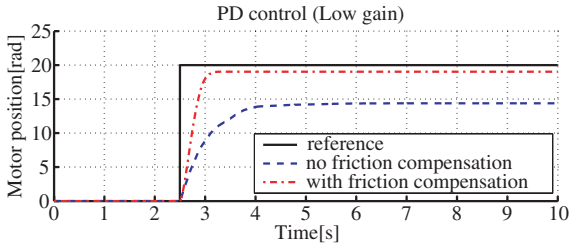


Fig. 10. Step responses with and without friction compensation in low servo stiffness.

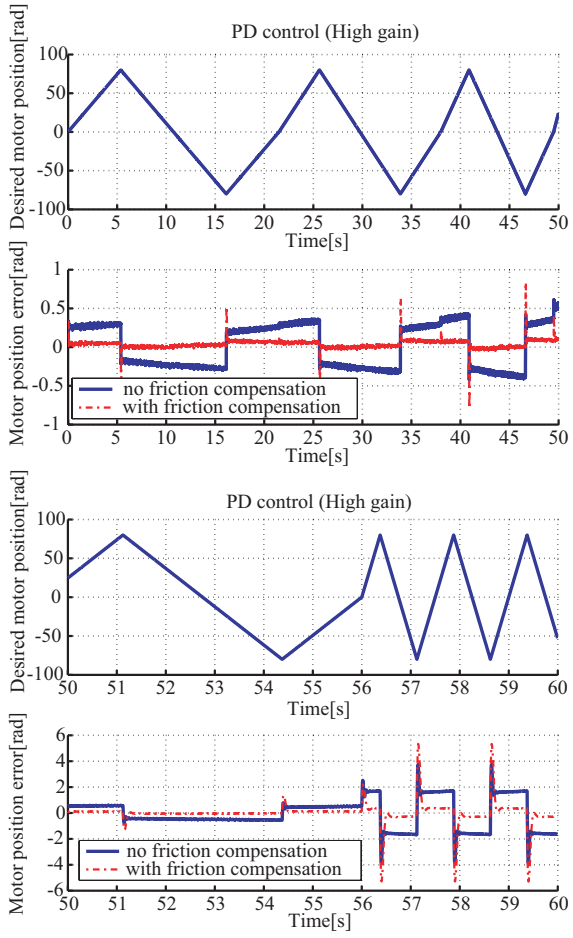


Fig. 11. Reference and errors of motor position with and without friction compensation.

,and $\tilde{u}_m$ is defined in the following:

$$\tilde{u}_m = \frac{\tilde{J}_m}{J_m} K_p \left(\theta_m^{ref} - \theta_m\right) - \frac{\tilde{J}_m}{J_m} K_d \dot{\theta}_m + \frac{1}{N}\tau_g \qquad (11)$$

Eq.9 means that the joint torque feedback reduces the motor inertia to $\tilde{J}_m$ for the system with new input $\tilde{u}_m$.

## IV. Evaluation Experiments

This section shows the experiments of the friction compensation and the joint torque feedback.

### A. Experiment system

The control system consists of the torque controlled joint (Fig. 5) and a link. The length of the link is 40(cm), and

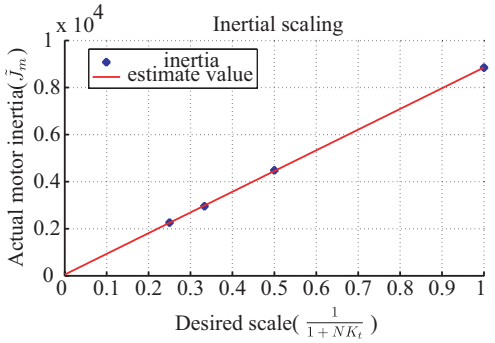


Fig. 12. Inertial scaling using torque feedback.

the link inertia $J_L$ is $2.08 \times 10^{-2}(\mathrm{kgm}^2)$. Motor angle is measured by an encoder (1000 counts per turn), and joint torque is measured by Torque Encoder. Motor velocity is calculated from the difference of the encoder. In addition, the control frequency of motor is 2(kHz).

### B. Experimental results of friction compensation

The controller in this experiment is a position control system consisting of PD control, gravity compensation and friction compensation without joint torque feedback in order to evaluate friction compensation. In this case, motor torque $\tau_m$ is given by

$$\tau_m = K_p(\theta_m^{ref} - \theta_m) - K_d\dot{\theta}_m + \frac{1}{N}\tau_g + \hat{\tau}_f \qquad (12)$$

The design parameter of the observer is $L = 30$. This controller is tested with two different experimental circumstance as follows.

1) **Exp. 1** : Reference angle of motor is a step input. $K_p = 2.9 \times 10^{-3}$ and $K_d = 6.1 \times 10^{-4}$ are assigned to evaluate the step response under low gain condition.
2) **Exp. 2** : Reference angle of motor is a triangle wave. $K_p = 1.2 \times 10^{-1}$ and $K_d = 1.5 \times 10^{-4}$ are assigned to evaluate the convergence performance of friction observer, when motor velocity changes drastically.

The results of Exp. 1 with and without friction compensation are shown in Fig. 10. The friction compensation is effective in a low gain condition, because the position error with friction compensation is smaller than that without friction compensation. Fig. 11 shows the results of Exp. 2 with and without friction compensation. When motor velocity changes drastically, the friction compensation is effective, because the position error with friction compensation is smaller than that without friction compensation.

### C. Experimental results of inertial scaling

In this subsection, we evaluate the proposed inertial scaling method. The control input $\tau_m$ is defined as follows:

$$\tau_m = K_t\left(\tau_g - \tau_t\right) + \frac{1}{N}\tau_g + \hat{\tau}_f \qquad (13)$$

The control input consists of the joint torque feedback, gravity compensation and friction compensation. Herein, we analyze the behavior of the joint. Substituting Eq. 1 and Eq.

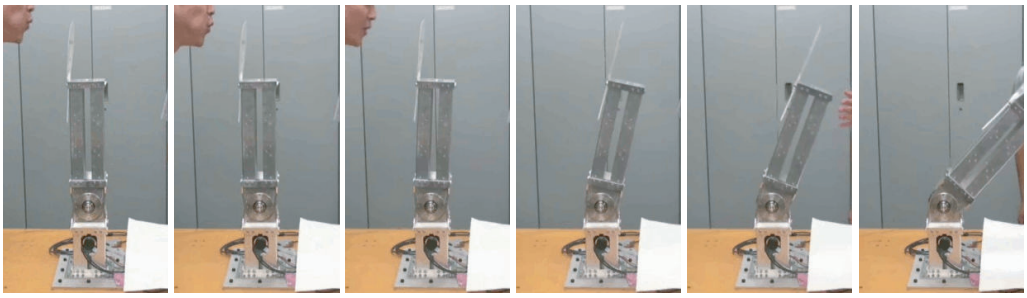

Fig. 13. Snapshots of blowing on the torque joint.

2 into Eq. 13, the dynamic equation at the link side is derived under the condition which is $\hat{\tau}_f = \tau_f$ and $\theta_m = N\theta_L$ in the following:

$$\left(\tilde{J}_m N^2 + J_L\right)\ddot{\theta}_L = \tau_{ext} \tag{14}$$

It is equal to behavior of a passive joint in freefall.

The virtual motor inertia was adjusted by changing the torque feedback coefficient $K_t$, and external force was applied to the joint. Fig. 12 shows the relationship between the desired motor inertia and the actual motor inertia which is calculated from Eq. 9. As the diagram indicates, it is found that the inertia scaling is efficient, because actual motor inertia corresponds with the desired value.

Then, Fig. 13 shows snapshots of falling the joint when we puffed air against the link. It is found from the result that the low impedance joint was realized by joint torque feedback and friction compensation.

## V. Conclusion

In this paper, we investigated the use of high resolution linear encoders, that have recently become available as a robotic component, for joint torque sensing.

1) The elastic body which is commonly introduced at the interface between a link and its drive system for strain gauges leads to low stiffness and bandwidth. It is usually not discussed that the local concentration of stress of such elastic components necessarily becomes the source of sensor hysteresis. The high resolution linear optical encoders are a recent technology and provide comparative sensitivity to strain gauges. It is a distinctive feature that the strain gauge sensing relies on local strain sensing though the encoder sensing measures the total sum of distributed strains or displacements. By making use of the feature we showed in this paper that the torque sensing of stiff joint drive system becomes possible using the high resolution linear encoders. The sensing system is free of electro magnetic noise that often limits the performance of strain gauge sensing.
2) Using this fabricated joint drive system using the high resolution linear encoder we experimentally confirmed that joint torque sensing was as accurate to 2.5% of full range.
3) We also designed the torque feedback controller based on the friction observer and experimentally confirmed the stiff torque feedback control, the low-impedance control against the external force, and the inertia shaping as low as one fourth of the original inertia.
4) The obtained results in this paper clearly show that torque sensing by use of high resolution linear optical encoders is a promising technology for building actively backdrivable joint drive systems for robots.


## Acknowledgement

The discussions with Dr. Christian Ott, the IRT Initiative, University of Tokyo and currently with DLR, Germany, were fruitful.


## References


[1] I. Godler, M. Hashimoto, and M. Horiuchi, "Performace of gain-tuned harmonic drive torque sensor under load and speed conditons," *IEEE/ASME Trans. on Mechatronics*, vol. 6, no. 2, pp. 155–160, 2001.

[2] D. Vischer and O. Khatib, "Design and development of high-performance torque-controlled joints," *IEEE Trans. on Robotics and Automation*, vol. 11, no. 4, pp. 537–544, August 1995.

[3] D. Tsetserukou, R. Tadakuma, H. Kajimoto, and S. Tachi, "Optical torque sensors for local impedance control realization of an anthropomorphic robot arm," *Int'l J. of Robotics and Mechatronics*, vol. 18, no. 2, pp. 121–130, 2006.

[4] G. Hirzinger, A. Albu-Schäffer, M. Hähnle, I. Schaefer, and N. Sporer, "On a new generation of torque controlled light-weight robots," *In Proc. of the IEEE Int. Conf. on Robotics and Automation*, vol. 4, pp. 3356–3363, May 2001.

[5] G. Zhang and J. Furusho, "Control of robot arms using joint torque sensors," *IEEE Control System Magazine*, vol. 18, no. 1, pp. 48–55, 1998.

[6] A. De Luca and R. Mattone, "Actuator failure detection and isolation using generalized momenta," *In Proc. of IEEE Int. Conf. on Robotics and Automation*, pp. 634–639, 2003.

[7] L. Tien, A. Albu-schäffer, A. Luca, and G. Hirzinger, "Friction observer and compensation for control of robots with joint torque measurement," *In Proc. of the IEEE Int. Conf. on Intelligent Robots and Systems*, pp. 3789–3795, 2008.

[8] A. Albu-Schäffer, C. Ott, and G. Hirzinger, "A unified passivity-based control framework for positionctorque and impedance control of flexible joint robots," *The International Journal of Robotics Research*, vol. 26, no. 1, pp. 23–39, 2007.

[9] K. Miyashita, T. Takahashi, S. Kawamata, S. Morinaga, and Y. Hoshi, "Non-contact magnetic torque sensor," *IEEE Transactions on Magnetics*, vol. 6, no. 2, pp. 1560–1562, 2001.

[10] S. Hirose and K. Yoneda, "Tri-axial force sensor using a split-type optical sensor," *Journal of Advanced Robotics*, vol. 5, no. 2, pp. 165–181, 1991.

[11] Y. Tsusaka, M. Koide, M. Tanaka, H. Nomura, and T. Kubo, "Development of a fast assembly robot arm with joint torque sensory feedback control," *In Proc. of the IEEE Int. Conf. on Robotics and Automation*, vol. 3, pp. 2230–2235, 1995.

[12] T. Kawakami, K. Ayusawa, H. Kaminaga, C. Ott, and Y. Nakamura, "Development of joint driving mechanism with rigid torque sensor and its torque control systems," *In Proc. of the 2008 JSME Conf. on Robotics and Mechatronics (In Japanese)*, pp. 1A1–B08, 2008.